

Photoluminescence Properties of Indium-doped ZnO/Cu-graphene Thin Films Synthesized by Hydrothermal Method

Yuanyuan Fan, Taotao Ai,* Wenhui Li, Zhifeng Deng, and Xinqiang Yuan

National and Local Joint Engineering Laboratory for Slag Comprehensive Utilization
and Environmental Technology, School of Materials Science and Engineering, Shaanxi University of Technology,
Shaanxi Hanzhong 723000, P.R. China

(Received January 18, 2019; accepted March 1, 2019)

Keywords: hydrothermal method, ZnO, nanostructure, photoluminescence properties, blue emission

Indium-doped ZnO/Cu-graphene thin films were successfully synthesized by a hydrothermal method at 90 °C for 6 h. The crystalline structure, elementary compositions, morphologies, and photoluminescence properties were investigated. The results indicated that ZnO nanorods with diameters varying from 0.315 to 3.348 μm were obtained on Cu-graphene flexible substrates. An ultraviolet (UV) peak at 398 nm and a blue band were observed on the room-temperature photoluminescent (PL) spectra. The UV emission peak mainly attributed to the exciton transition. The blue emission band was assigned to the Zn interstitial (Zni) and Zn vacancy (VZn) level transition. The strongest blue emission band was observed on the PL spectra corresponding to the indium (In) doping concentration of 0.3%. The influence of In doping on the blue band was also investigated.

1. Introduction

Zinc oxide (ZnO) is a II-VI wide-band-gap semiconductor ($E_g = 3.37$ eV), and its exciton binding energy (60 meV) is much higher than the thermal ionization energy (26 meV) at room temperature.⁽¹⁾ Therefore, an effective visible and ultraviolet emission can still be achieved at room temperature, which is known as an ideal material for a light-emitting device. Furthermore, the ultraviolet light emission of ZnO thin films has always been the focus of attention, and the mechanism has become a consensus. At present, people pay more attention to the blue-green light emission characteristics of the films, so that they can be used as blue fluorescent materials in the field of flat-panel displays or short-wavelength light-emitting diodes.^(2,3) Zhang *et al.* reported the fabrication of high-brightness n-ZnONWs/p-GaN film hybrid heterojunction light-emitting diode (LED) devices by directly growing n-type ZnO nanowire arrays on p-GaN wafers.⁽⁴⁾ However, we found that most ZnO-based light emitting devices use conventional substrates such as GaN, Al₂O₃ and Si, but heat dissipation cannot be well solved, causing the performance degradation of the devices. During the past decades, ZnO-based flexible thin

*Corresponding author: e-mail: aitaotao0116@126.com
<https://doi.org/10.18494/SAM.2019.2302>

films were attracting significant attention and considered as the most prominent candidate for next-generation flexible devices systems.⁽⁵⁻⁷⁾ In our work, Cu foil is used as a substrate in ZnO-based light-emitting devices, which is known as an ideal choice owing to its high thermal conductivity.⁽⁸⁾ Moreover, owing to good photoelectronic performance, graphene (GR) can be used as an ideal electron collector for the efficient collection of photogenerated electrons and can affect the electron transport effectively. Therefore, we chose commercial Cu foil coated with a graphene film as the substrate to prepare flexible electronic devices. Usually, the properties of ZnO can be improved by doping with some metal elements, such as Group III elements (Al, Ga, and In).⁽⁹⁻¹¹⁾ Among them, the blue emission of In-doped ZnO can be enhanced to better meet practical application requirements. Zebbar *et al.* found that less resistive In-doped ZnO (ZnO:In) thin films mainly exhibited a blue visible emission at room temperature.⁽¹²⁾ In our studies, In-doped ZnO thin films grown on Cu-graphene (Cu-GR) flexible substrates were hydrothermally synthesized by introducing a trace amount of indium nitrate hydrate [$\text{In}(\text{NO}_3)_3 \cdot 4.5\text{H}_2\text{O}$] to zinc nitrate hexahydrate [$\text{Zn}(\text{NO}_3)_2 \cdot 6\text{H}_2\text{O}$] and hexamethylenetetramine ($\text{C}_6\text{H}_{12}\text{N}_4$, HMTA), and the photoluminescence properties of the composite structure were studied. Our studies can provide a theoretical basis for the application of ZnO-based devices in the field of short-wavelength optoelectronics.

2. Experimental Section

2.1 Synthesis of samples

In-doped ZnO nanostructures grown on Cu-GR were prepared by a hydrothermal method. Zinc nitrate hexahydrate [$\text{Zn}(\text{NO}_3)_2 \cdot 6\text{H}_2\text{O}$] (0.5 M/L) and $\text{C}_6\text{H}_{12}\text{N}_4$ (0.5 M/L) were dissolved in deionized water to prepare a precursor aqueous solution of 30 mL, and $\text{In}(\text{NO}_3)_3 \cdot 4.5\text{H}_2\text{O}$ with concentrations of 0, 0.1, 0.3, 0.5, and 0.7% (the doping concentration of 0.7% was 0.007 M/L) was added to the mixed solution. The reaction solution was stirred for 30 min and then transferred to high-pressure reactors. The ZnO seed layer was sputtered onto a Cu-graphene substrate for 130 s using ion sputtering equipment under a sputtering current of 10 mA and a vacuum of 10 Pa. The main purpose of sputtering the seed layer instead of using the solution process is to promote ZnO growth more easily during the hydrothermal process and further improve adhesion between the ZnO layer and the substrate. The thickness of the ZnO seed layer obtained by sputtering is about 4 nm. The substrate adhered to the ZnO seed crystal was sandwiched with a specimen holder and placed vertically into an autoclave, which was completely submerged in the as-prepared mixed solution. The reactor was sealed, placed in an electric oven, and heated at 90 °C for 6 h.

2.2 Characterization

The crystalline structure of the material was obtained by X-ray diffraction (XRD) analysis with Cu-K α radiation of wavelength $\lambda = 0.15418$ nm (Rigaku, IV X-ray diffractometer). X-ray photoelectron spectroscopy (XPS) measurements were performed on an ESCALAB 250Xi

spectrometer (excitation source of Al K α , 1486.6 eV) to study the composition and chemical state of the sample surface. The morphology of the samples was characterized by scanning electron microscopy (SEM) (JEOL, JSM-6700F). Photoluminescence (PL) spectra were measured using a fluorescence spectrometer (Edinburgh Instruments FLS 980) at an excitation wavelength of 320 nm.

3. Results and Discussion

3.1 Crystalline structure and elemental compositions of the samples

The XRD patterns of IZO/Cu-GR thin films with different In doping concentrations are shown in Fig. 1(a). The labeled peaks are all characteristic peaks of ZnO, except for the three diffraction peaks at 44.1, 52, and 74.3° that are attributed to the Cu-GR substrate. The XRD peak of the flexible Cu-GR substrate material is shown in Fig. 1(b). The peak positions of the pure and doped ZnO samples are in conformity with the Joint Committee on Powder Diffraction Standards (JCPDS) card (No. 36-1451), verifying the hexagonal wurtzite structure of the products.

According to the interplanar spacing formula [Eq. (1)], the hexagonal system can be used to calculate the lattice constant of the sample.

$$d = \frac{a}{\sqrt{\frac{4}{3}(h^2 + hk + k^2) + l^2 \frac{a^2}{c^2}}} \quad (1)$$

Here, d represents the interlayer spacing between adjacent lattice planes of ZnO and (hkl) are the Miller indices of the crystal plane. The stress formula [Eq. (2)] of the hexagonal lattice based on the biaxial strain model can be applied to estimate the stress along the c-axis of the ZnO films.

$$\sigma = \frac{2c_{13}^2 + c_{33}(c_{11} + c_{12})}{2c_{13}} \times \frac{c - c_0}{c_0} = -233 \frac{c - c_0}{c_0} \text{ (GPa)} \quad (2)$$

In Eq. (2), the elastic constants c_{ij} of single-crystal ZnO are fixed values, which are $c_{11} = 208.8$, $c_{12} = 119.7$, $c_{13} = 104.2$, and $c_{33} = 213.8$, and all measured in GPa. σ denotes the stress in the film. c and c_0 are the c-axis lattice constants of the ZnO film and complete crystal, respectively. The lattice constant of the flexible Cu-GR substrate material is calculated as $a = 3.6209$ Å through the function of Jade 6. The lattice mismatch between the substrate and ZnO is about 11.4%. The lattice constants and magnitudes of the stress of IZO/Cu-GR thin films are listed in Table 1. As can be seen clearly, with increasing In doping concentration, the lattice constants of IZO/Cu-GR thin films first increase and then decrease; this due to the substitution or interstitial doping of In atoms, as well as the bending deformation of the flexible substrate, causing the internal stress of ZnO crystals to change and then giving rise to lattice distortion.

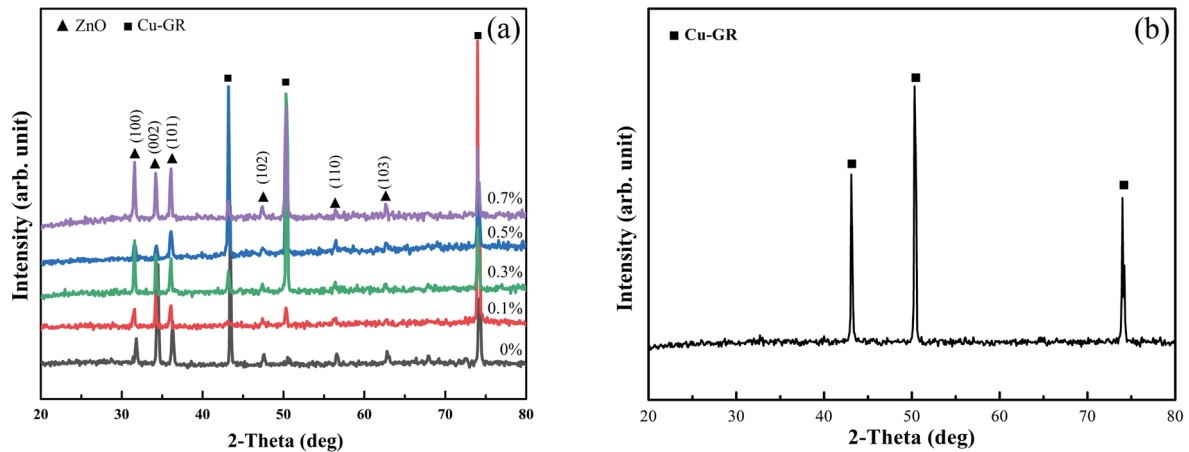


Fig. 1. (Color online) (a) XRD patterns of In-ZnO/Cu-GR thin films with different In doping concentrations and (b) XRD peak of the flexible Cu-GR substrate material.

Table 1

Lattice constants and stress magnitudes (σ) of In-ZnO/Cu-GR thin films.

In doping concentration (%)	Lattice constant (only c) (\AA)	σ (GPa)
0.0	5.2144	-0.34906
0.1	5.2157	-0.40723
0.3	5.2178	-0.50121
0.5	5.1936	0.5103
0.7	5.2140	-0.4028

XPS measurements have been further conducted to investigate the surface composition and chemical states of the elements in the IZO/Cu-GR thin films, as shown in Fig. 2. The strong photoelectron peaks corresponding to Zn, O, and C elements can be clearly seen on the XPS survey spectrum. The C 1s peak was attributed to the surface of the sample absorbing a handful of CO₂ in air. The peak of In 3d (~443.58 eV) is not observed at the relevant positions in the survey spectrum, which is mainly because the incorporation of In atoms and its scattering cross section are small. The high-resolution XPS spectra of Zn and O elements are shown in Figs. 2(b) and 2(c), respectively. The two peaks at 1021.64 and 1044.76 eV in the high-resolution spectrum [Fig. 2(b)] of the photoelectron peak corresponding to Zn 2p are attributed to Zn 2p_{3/2} and Zn 2p_{1/2}, respectively, indicating that the elemental zinc existed mainly as Zn²⁺, which proves that most of the Zn elements in the IZO/Cu-GR exhibit positive divalent oxidation states. Figure 2(c) shows the high-resolution XPS spectrum of oxygen. As clearly seen in Fig. 2(c), the O 1s level peaks for the ZnO nanowires have asymmetric shapes, which can be fitted by two nearly Gaussian peaks centered at 530.50 and 531.58 eV; the peak with a low binding energy of ~530.50 eV corresponds to O²⁻ ions in the wurtzite structure of ZnO, whereas the peak with a high binding energy of ~531.58 eV can be attributed to O²⁻ in the oxygen-deficient regions in the ZnO matrix, such as oxygen-deficient defects and impurities.⁽¹³⁾

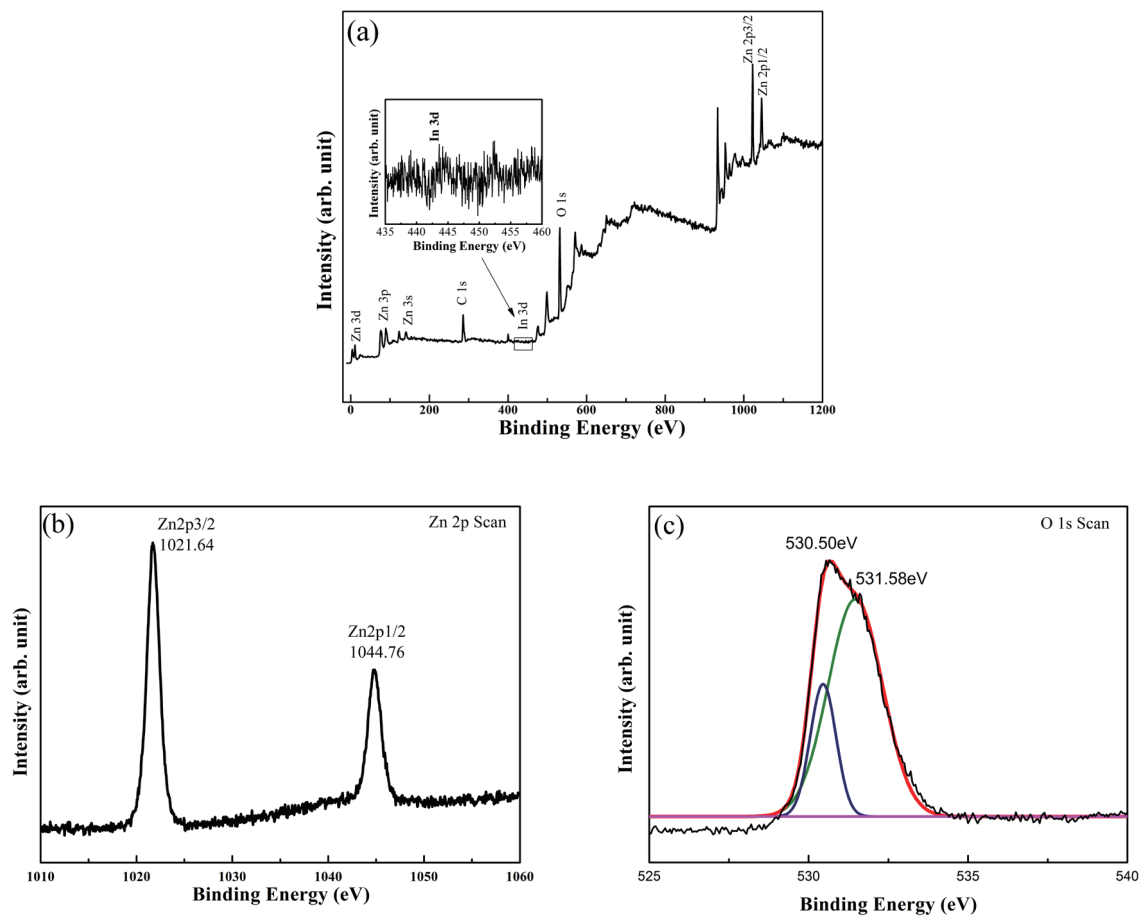


Fig. 2. (Color online) XPS survey spectra of 0.7%In-ZnO/Cu-GR films, (a) XPS survey scan spectrum, the inset of which corresponds to the photoelectron peak of In 3d, and (b and c) high-resolution spectra at Zn 2p and O 1s state energies, respectively.

3.2 Morphologies

To investigate the effect of In content on the morphological evolution of ZnO, SEM images of the samples doped with different In concentrations (0, 0.1, 0.3, 0.5, and 0.7%) are presented in Fig. 3. As can be seen in Fig. 3, all samples present a significant nanorod-like structure with an inerratic hexagonal cross section, and most of the ZnO nanorods (NRs) grow with an irregular arrangement rather than completely perpendicular to the substrate, which is generated by the presence of stress in the flexible substrate. As the level of In doping increases from 0 to 0.7%, the diameters of IZO NRs increase gradually, ranging from 0.315 to 3.348 μm .

3.3 Room-temperature PL properties

Figure 4 shows the room-temperature PL spectra from 350 to 800 nm. The PL spectra of all films reveal a luminescence behavior with a weak and narrow ultraviolet (UV) emission at ~ 398

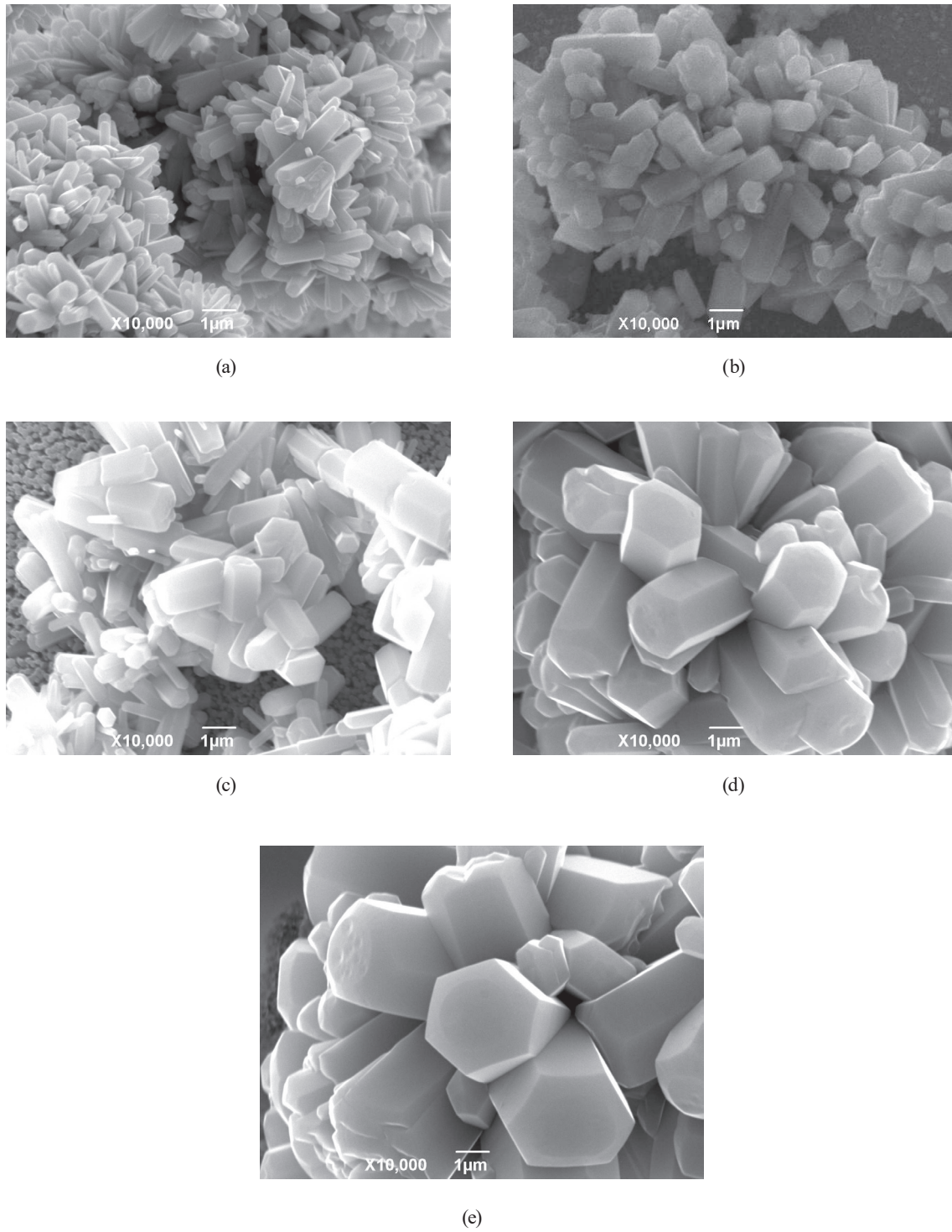


Fig. 3. SEM images of IZO nanostructures grown on Cu-GR substrate at different In doping concentrations: (a) 0, (b) 0.1, (c) 0.3, (d) 0.5, and (e) 0.7%.

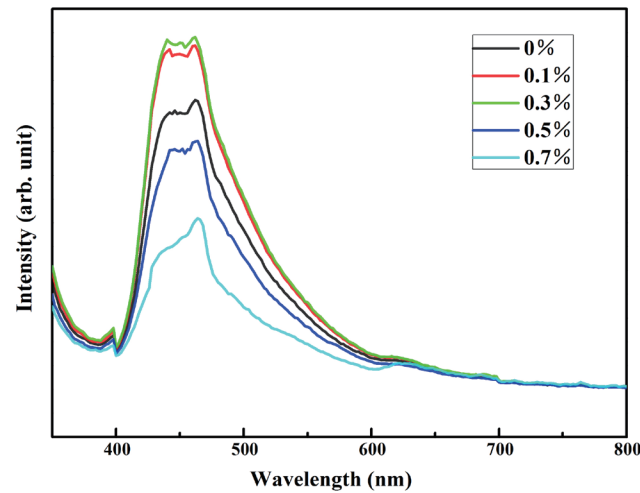


Fig. 4. (Color online) Room-temperature PL spectra of IZO/Cu-GR with different In doping

(3.12 eV) nm and blue double peaks located at 443 nm (2.80 eV) and 462 nm (2.68 eV). From Fig. 4, it can be seen that I_{vis} is significantly larger than I_{uv} , and that the blue luminescence region is the main emission. The UV emission peak is related to the recombination of excitons, which can be explained by the near-band-edge transition of ZnO NRs. However, the UV emission intensity in this work does not change clearly with the increase in In content, so In doping has little effect on UV emission. We can explain the wide blue emission band by the electronic structure analysis of ZnO intrinsic point defects.^(14,15) Using the full-potential linear muffin-tin orbital method, Xu *et al.* calculated the energy levels of the intrinsic defects in ZnO films.⁽¹⁶⁾ The energy interval from the bottom of the conduction band to the VZn level was about 3.06 eV and the energy interval from the Zn_i level to the top of the valence band was about 2.88 eV, which was consistent with the energies of the double peaks at 443 and 462 nm. Therefore, the blue emission band was assigned to the electron transition from both the bottom of the conduction to the VZn levels and the Zn_i level to the top of the valence band. As the level of In doping increases, the intensity of the blue emission increases and the 0.3%In-ZnO/Cu-GR film has the highest blue emission intensity, which may cause the implanted In³⁺ ions to form the impurity levels in the ZnO layer to broaden the blue emission range and enhance the blue emission capacity. After the level of In doping reaches 0.5%, more In³⁺ ions would contribute to the decrease in defect concentration, forming a weak blue band.

4. Conclusions

IZO/Cu-GR thin films were successfully fabricated by a low-temperature hydrothermally assisted ion sputtering method. In atoms were successfully incorporated into ZnO and affected the growth morphology of ZnO. As the level of In doping increased, the diameter of ZnO NRs increased, ranging from 0.315 to 3.348 μm . The mechanism of luminescence was discussed in

that the blue emission band was assigned to the electron transition from both the bottom of the conduction to the VZn levels and the Zn_i level to the top of the valence band. The strongest blue emission band was observed on the PL spectra when the level of In doping was 0.3%. The appearance of the blue peak is important for the development and application of ZnO-based blue emission devices.

Acknowledgments

This work was supported by the National Natural Science Foundation of China (Grant No. 51671116), the Project Supported by the Key Project of the Natural Science Basic Research Plan in Shaanxi Province of China (Grant No. 2016JZ016), and the Scientific Research Startup Program for Introduced Talents of Shaanxi University of Technology, China (Grant No. SLGQD1801).

References

- 1 S. Sepulveda-Guzman, B. Reeja-Jayan, E. D. L. Rosa, A. Torres-Castro, V. Gonzalez-Gonzalez, and M. Jose-Yacamán: *Mater. Chem. Phys.* **115** (2009) 172. <https://doi.org/10.1016/j.matchemphys.2008.11.030>
- 2 J. Y. Zhang, H. B. Feng, W. C. Hao, and T. M. Wang: *J. Sol-Gel. Sci. Technol.* **39** (2006) 37. <https://doi.org/10.1007/s10971-006-9416-1>
- 3 Z. P. Wei, Y. M. Lu, D. Z. Shen, Z. Z. Zhang, B. Yao, B. H. Li, J. Y. Zhang, D. X. Zhao, X. W. Fan, and Z. K. Tang: *Appl. Phys. Lett.* **90** (2007) 042113. <https://doi.org/10.1063/1.2435699>
- 4 X. M. Zhang, M. Y. Lu, Y. Zhang, L. J. Chen, and Z. L. Wang: *Adv. Mater.* **21** (2009) 2767. <https://doi.org/10.1002/adma.200802686>
- 5 C. P. Liu, H. E. Wang, T. W. Ng, Z. H. Chen, W. F. Zhang, C. Yan, Y. B. Tang, I. Bello, L. Martinu, W. J. Zhang, and S. K. Jha: *Phys. Status Solidi B* **249** (2012) 627. <https://doi.org/10.1002/pssb.201147393>
- 6 W. Wang, T. T. Ai, W. H. Li, R. Jing, Y. H. Fei, and X. M. Feng: *J. Phys. Chem. C* **121** (2017) 28148. <https://doi.org/10.1021/acs.jpcc.7b08181>
- 7 E. Fortunato, P. Barquinha, and R. Martins: *Adv. Mater.* **24** (2012) 2945. <https://doi.org/10.1002/adma.201103228>
- 8 W. X. Huo, Z. X. Mei, M. L. Zhao, Y. X. Sui, B. Zhao, Y. H. Zhang, T. Wang, S. J. Cui, H. L. Liang, H. Q. Jia, and X. L. Du: *IEEE Trans. Electron. Devices* **65** (2018) 3791. <https://doi.org/10.1109/TED.2018.2859277>
- 9 G. D. Yuan, W. J. Zhang, J. S. Jie, X. Fan, J. X. Tang, I. Shafiq, Z. Z. Ye, C. S. Lee, and S. T. Lee: *Adv. Mater.* **20** (2008) 168. <https://doi.org/10.1002/adma.200701377>
- 10 L. P. Peng, L. Fang, X. F. Yang, Y. J. Li, Q. L. Huang, F. Wu, and C. Y. Kong: *J. Alloys Compd.* **484** (2009) 575. <https://doi.org/10.1016/j.jallcom.2009.04.139>
- 11 S. Y. Kuo, W. C. Chen, F. I. Lai, C. P. Cheng, H. C. Kou, S. C. Wang, and W. F. Hsieh: *J. Cryst. Growth* **287** (2006) 78. <https://doi.org/10.1016/j.jcrysgro.2005.10.047>
- 12 N. Zebbar, L. Chabane, N. Gabouze, M. Kechouane, M. Trari, M. S. Aida, S. Belhousse, and F. Hadj Larbi: *Thin Solid Films* **605** (2016) 89. <https://doi.org/10.1016/j.tsf.2015.09.061>
- 13 K. C. Barick, M. Aslam, and D. Bahadur: *J. Alloys Compd.* **587** (2014) 282. <https://doi.org/10.1016/j.jallcom.2013.10.206>
- 14 M. H. Lee, Y. C. Peng, and H. C. Wu: *J. Alloys Compd.* **616** (2014) 122. <https://doi.org/10.1016/j.jallcom.2014.07.098>
- 15 R. Saniz, Y. Xu, M. Matsubara, M. N. Amini, H. Dixit, D. Lamoén, and B. Partoens: *J. Phys. Chem. Solids* **74** (2013) 45. <https://doi.org/10.1016/j.jpss.2012.07.017>
- 16 P. S. Xu, Y. M. Sun, C. S. Shi, F. Q. Xu, and H. B. Pan: *Sci. China, Ser. A* **44** (2001) 1174. <https://doi.org/10.1007/BF02877436>